

# Effect of acetic acid on amorphous carbon removal along a CNT synthesis reactor

A. A. KHODADADI, M. MAGHREBI\*, Y. MORTAZAVI<sup>a</sup>, A. SANE,  
Y. SHIRAZI, M. RAHIMI, Z. TSAKADZE<sup>b</sup>, S. MHAISALKAR<sup>b</sup>

*Catalysis & Nanostructured Lab, School of Chemical Engineering, University of Tehran, Tehran, Iran*

*<sup>a</sup>Nanoelectronics Centre of Excellence, University of Tehran, POB 11365-4563, Tehran, Iran*

*<sup>b</sup>School of Materials Science and Engineering, Nanyang Technological University, Singapore 639798, Singapore*

The mm-long carbon nanotubes (CNTs) arrays were grown in a xylene-ferrocene reactor, and subjected to extensive characterization in different longitudinal positions of reactor and upon addition of small amount of acetic acid. Through optical microscopy, Raman spectroscopy, FESEM, XRD and HRTEM characterizations, it was consistently revealed that acetic acid alleviates amorphous carbon layer, which gradually thickens CNTs along the reactor. The added acetic acid also resulted in higher growth rate along the so-called growth window. HPLC of extracted byproducts confirmed the presence of some polycyclic aromatic hydrocarbons. The solid weight of these byproducts decreased upon addition of catalyst precursor, as well as acetic acid to pure xylene feed. The results suggest that primary light products of xylene pyrolysis can be competitive feeds for both catalytic and subsequent pyrolytic reactions. They may also be more efficient feeds for CNTs growth than xylene itself.

(Received October 16, 2009; accepted November 12, 2009)

*Keywords:* Carbon nanotubes, mm-long array, Longitudinal study of reactor, Growth window, Acetic acid, Amorphous carbon

## 1. Introduction

Carbon nanotubes (CNTs) are novel materials well-known for their extraordinary aspect ratio and exotic properties [1-3]. They are mostly synthesized through various chemical vapor deposition (CVD) methods. One of the recent branches of CVD is floating catalyst method. In this method an organometallic substance, usually metallocenes, enters continuously along with a hydrocarbon and a carrier gas to instantly produce metal nanoparticles, which then catalyze the CNTs synthesis. Though the reactants are relatively inexpensive, the process is not still cost-effective and heavily depends upon the labor work [4]. Therefore, to have a more economically viable production, an optimized synthesis reaction is desired.

It has been suggested that the CNTs growth may be limited due to inhibitions caused by excess amorphous carbon [5] or in-situ made iron carbide [6, 7].

Traditionally, researchers use hydrogen in carrier gas to remove/alleviate deposition of the amorphous carbon [8]. However, there are few recent researches, which successfully employed oxygen or oxygen-containing species to remove byproducts: It was shown that slight amount of gaseous oxygen can boost the CNTs growth significantly, turning the entangled nanotubes to large dense arrays. However, oxygen is hard to control and just slightly more amount of it can diminish the growth completely [9]. The CO<sub>2</sub> gas was also suggested to help catalytic growth of CNTs through inhibiting amorphous carbon deposition [10, 11].

Nonetheless, the liquid additives are visibly more desired than gaseous ones, as they don't need an independent flow meter, and can simply be incorporated to injected feedstock in desired concentrations. There are some reports about efficient growth of CNTs, using oxygenates, like ethanol [12, 13] and camphor [14, 15], instead of common feed stock. While the results were promising, one can not compare the results in term of oxygen content, because of different employed operational parameters. As a matter of fact, the floating catalyst is so sensitive/complicated process that one may reach opposite results upon substitution of hydrocarbon feedstock [16, 17]. In this study, we used few mole percent of acetic acid in a common hydrocarbon, to provide growth conditions as similar as possible. While acetic acid is an inexperienced reactant in the field of CNTs synthesis, its effect may be considered analogous to that of CO<sub>2</sub>. It is known that acetic acid gradually converts to CO<sub>2</sub> at elevated temperatures [18].

Furthermore, to have more exhaustive image of reactor, we conducted a point-to-point longitudinal investigation of CNT products, extended throughout the so-called *growth window* (GW) [19]. It has been found just recently, that quality variation of CNTs array could be significant along the GW [20].

## 2. Experimental

The experimental setup used in this study to synthesis carbon nanotubes by floating catalyst method comprised a feeding and a reactor system. The feeding system included

a syringe pump for injection of 0.2-0.5 ml/min of feed solution. The liquid feeds were the solutions of xylene, which contained 0.1 g/ml of ferrocene, as well as 0.0, 1.0, and 2.0 mole percent of acetic acid (naming AA0, AA1 and AA2 respectively).

A mass flow controller was used to introduce 300-700 sccm of argon as carrier gas through the reactor. A 21.7 mm ID, 100 cm long quartz tube reactor was placed in a two-zone furnace. The first zone at the entrance of the reactor and the following second zone were heated to 300 and 850°C, respectively. The temperature in the annular region between the reactor and furnace tubes along the system was monitored during the CNTs synthesis. The liquid feed was evaporated in the first zone. An ice-water cooled condenser was used to trap heavy byproducts. A 4.0 mm OD, 25.0 cm long quartz rod at the center of the second zone of the reactor was used as a substrate for CNTs growth

Following the injection of 10 ml of xylene solution, the reactor was cooled to room temperature under the Ar atmosphere. The samples of CNTs arrays collected at specific longitudinal positions, and were characterized by optical microscopy (Olympus BX 51), micro-Raman spectroscopy (WITec TS-150), and field emission scanning electron microscope (Jeol JSM 6340F). Some selected CNTs samples were also characterized by X-ray diffraction (Shimadzu 6000) as well as high resolution transmission electron microscopy (JEM-2010F).

The optical microscope was used to measure the CNTs arrays heights along the CNTs growth zone on the quartz rod. The micro-Raman was operated with a 488 nm laser of 1.2  $\mu\text{m}$  spot size with an acquisition time of 30.0 s, and a laser power of 3.0 mW. Raman spectra for at least 6 different positions of CNTs sample on each piece of the quartz rod were obtained. X-ray diffraction studies were employed overnight (0.1°/min scan rate), under 50 kV and 50 mA working conditions. For TEM, a sample of CNTs arrays was dispersed in acetone by 90 min sonication, and the suspension was then applied on the carbon-coated copper grid. For all employed characterizations (except XRD), CNTs arrays have been studied from the side view, preferentially in the height middle of array, to disregard likely irregular/amorphous structures in the top/bottom of array (not published yet).

We also collected the yellow-brownish tar-like substances which condensed in the cool end of reactor as well as water-cooled steel condenser. They were washed by dichloromethane, and then were extracted through overnight vacuum drying. The resultant solid residues were weighed and re-solublized in acetonitrile. HPLC measurements were done on a HP Agilent 1100 equipped with a 4.6 $\times$ 250 mm ZORBAX Eclipse C-18 column (particle size: 5 $\mu\text{m}$ ). The HPLC method employed on each

sample was as follows: injection volume of 20 $\mu\text{l}$ , wavelength detection at 254 nm, and acetonitrile : water (60/40 v/v) as mobile phase at 1 ml/min for 120 min. Through all the handlings and experiments, these materials were protected in UV-shielding bottles and cool environments. The HPLC spectra qualitatively compared with the standard mixture of polycyclic aromatic hydrocarbons (PAHs) in acetonitrile (Supelco, catalog no. 47940-U).

### 3. Results and discussion

#### 3.1. CNTs array's height profiles

Fig. 1(a) depicts typical results of optical microscopy, showing height profile of the CNTs arrays along their GWs. Due to difficulties of determining height of extra-short CNTs arrays, we considered the arrays just longer than  $\sim$ 0.3 mm formed in the GWs.

Fig. 1(b) illustrates the longitudinal position of pre-heater and main furnace, as well as GW of AA0 sample with regards to temperature profile. As can be seen, the CNTs arrays begin to grow around 750°C which corresponds to the longitudinal position of 35cm. However, the growth of CNTs arrays is terminated after 10 cm at the temperature of about 840°C, before reaching the maximum temperature of the reactor. All the growth profiles exhibit height maxima near each other.

Regarding the initial increase in the arrays' heights, one may relate it with an increase in both temperature and residence time, the so-called "equivalent residence time" (ERT) [21]. The increased equivalent residence time can facilitate endothermic deposition reactions, which result in an increased carbon supply, as well as more dissolution/diffusion of carbon into the catalyst [22]. These in turn may improve the overall growth process. Similarly, the following reduction in the heights of the arrays shall be attributed again to the prolonged ERT, which may enhance pyrolytic reactions lead to unwanted byproducts. In fact, precursors of CNTs are unstable at higher temperatures and result to excessive deposition of amorphous carbon, which covers the surface of catalyst. Such passivated catalyst surface may lead to less catalytic growth and so less CNTs array heights.

AA1 and AA2 have relatively larger array heights along the GW compared to those of AA0. The maximum array height of AA2 is  $\sim$ 17% longer than that of AA0. Similarly, the weight of CNTs products of AA2 was revealed to be  $\sim$ 22% higher than that of AA0. Thus, one can conclude that acetic acid has a positive effect on the total growth rate averaged along the GW.

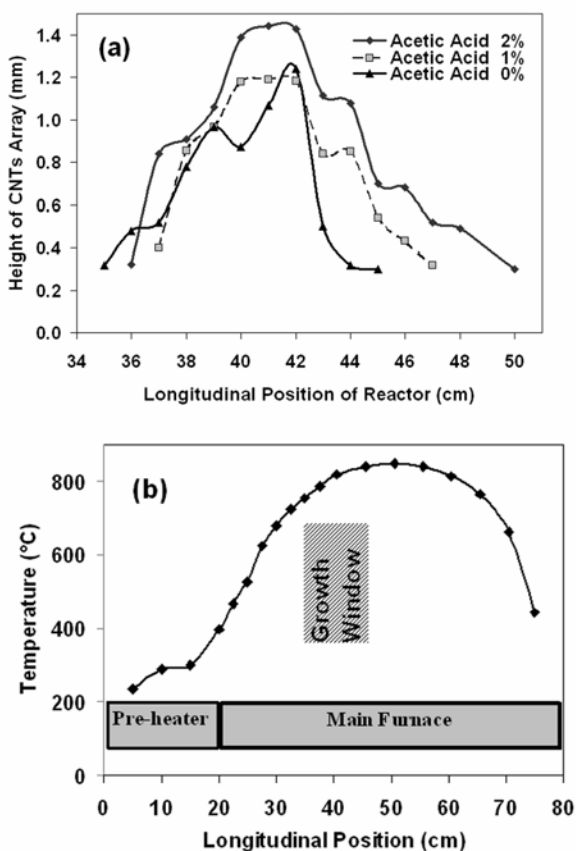


Fig. 1 (a) The detailed topography of CNTs arrays along the reactor, measured by optical microscopy, corresponding to AA0, AA1, and AA2 samples. (b) The temperature profile of reactor, showing the typical longitudinal position of pre-heater, main furnace and GW for the case of AA0.

In contrast to acetic acid-containing samples, AA0 profile exhibits a small peak and valley prior to its main peak. Unexpectedly, this pattern was reproducible for AA0 sample in several successive runs. We suggest that this peculiar growth profile can be considered as two adjacent ones: primary and secondary regimes. The former may relate to direct adsorption/dissolution of primary hydrocarbon feed (i.e., xylene). This planar molecule needs several adjacent sites with a proper geometry on the catalyst to be adsorbed on them and further react to produce CNTs [23]. At longer ERT, the chance of catalytic decomposition of xylene increases, which in turn may limit the amount of proper catalyst ensembles for effective adsorption of xylene. This pseudo-shortage of catalyst active sites may lead to accumulation of adsorbed hydrocarbon on catalyst surface, acting as a catalytic inhibitor [24]. This may explain the primitive drop of CNTs array height before the main height maximum. On the other hand, the longer ERT can also increase the chance of the thermal decomposition of xylene. It was predicted that pyrolysis of xylene primarily results in  $C_2$

hydrocarbons, which can later on develop to PAHs [25]. The development of former at the middle of GW may be responsible for the height rise of CNTs arrays for a second time. These smaller molecules have more chance to find free adsorption sites on the catalyst surface, and can well compete with the primary feed on utilizing the catalyst surface at larger ERTs. In fact,  $C_2$  hydrocarbons, such as ethylene [26] and specially acetylene [27] are promising/well-known hydrocarbon feeds in CVD growth of CNTs.

Though one can see small shoulders prior to the main peaks of AA1 and AA2 profiles, they are not so clear. As will be discussed later, acetic acid alleviates amorphous carbon, and so the resultant catalyst deactivation. This may compensate the saturation of catalyst surface, and can hide the small abovementioned drop in CNTs growth rate around the middle of GW for AA1 and AA2 samples.

### 3.2. Morphology variation along the GW

Figs 2(a-c) illustrate typical FESEM images of AA0 sample in different longitudinal positions. While CNTs are relatively thin and well-ordered at the beginning of GW (Fig. 2(a)), they gradually lose their quality/order, obtaining bumpy surface (Fig. 2(b)). The thickening with irregular coating is so severe near the end of GW, that it seems some tubes are partially consolidated (Fig. 2(c)). One can also observe some CNTs tips partially peeled from a thick coating, showing more brittleness of the latter. In fact, the common mechanical/thermal stresses during handling the samples, can apply some strains, in which different materials show different strengths: While graphitic CNTs are well-known for their extra-high tensile and torsional strength [28], amorphous carbon is more vulnerable [29]. Thus, the latter is more susceptible to breakage. Furthermore, the gradual addition of amorphous carbon may reduce the flexibility of resultant composite tubes. So, the less flexible tubes have lower tendency to obey Van der Waals forces, which are supposed to be responsible for alignment of the arrays [30, 31].

Similar to AA0 sample, AA2 samples showed similar trend in quality worsening and thickening along the GW, but with slower pace (Fig. 2(d-f)). While AA0 and AA2 samples have relatively similar morphologies at the beginning of GW, the latter can keep its order and neatness more than the former toward the end of GW. Again the relatively higher alignment of AA2 may be attributed to its lower amorphous content.

Our detailed microscopy observations revealed a continuous trend toward higher diameters for all CNTs samples throughout the GW, while acetic acid supplement decelerate this trend significantly (Fig. 3). This finding may be related to thickness of an amorphous overcoat, which increases along the GW. One can also relate the gradual rising of amorphous carbon to gradual decline in height of CNTs arrays around the end of GWs (Fig. 1(a)). This suggests amorphous carbon may be responsible for the inhibition of catalytic reactions and the drop in growth rate.

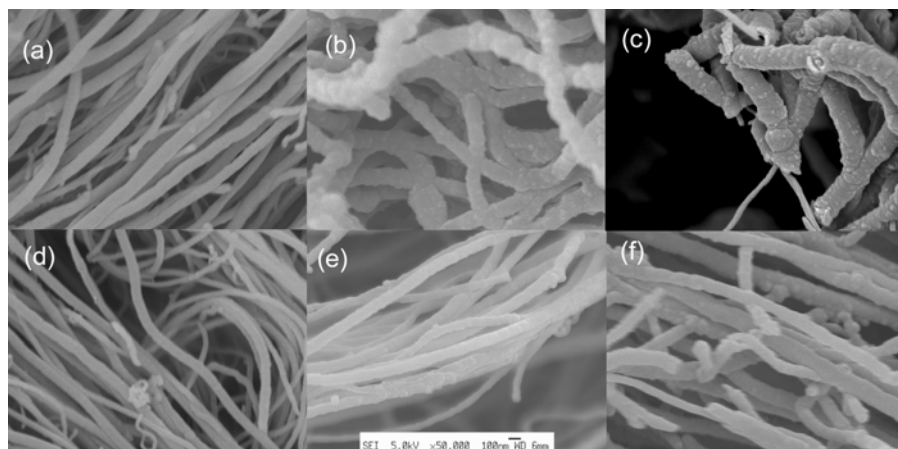


Fig. 2 FESEM images depict morphology of CNTs arrays respectively at the beginning, middle, and end of GW of AA0 sample (a-c), comparing them with counterpart points from AA2 sample (d-f)

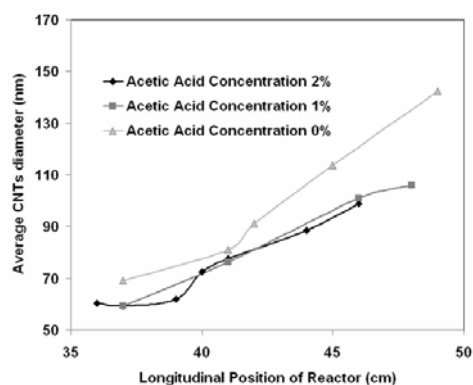


Fig. 3 Detailed variation of averaged diameter of CNTs along the GW of AA0, AA1, and AA2 samples, based upon FESEM results

### 3.3. Variation of amorphous/imperfect species

Raman spectra of AA0 sample at various axial positions are presented in Fig. 4(a), showing characteristic D- and G-bands around  $1380$  and  $1580$   $\text{cm}^{-1}$  respectively. As shown, one can see the relative increase of D- to G-band along the GW, presenting more amorphous/imperfect structures near the end of growth profile.

Fig. 4(b) depicts the averaged  $I_D/I_G$  results, calculated from Raman spectroscopy of all samples along the reactor. Evidently, the general trend for the all samples reveals an increase in  $I_D/I_G$  of carbon products along the GWs. This shows continuous rising of amorphous/imperfect structures along the GWs, due to the instability of CNTs precursors, leading to deposition of large amounts of carbonaceous compounds rather than graphitic CNTs. Nonetheless, acetic acid lowers the deposition of amorphous/imperfect structures; while all the samples have near the same  $I_D/I_G$  ratios at the beginning of GW, the higher amount of acetic acid, the lesser  $I_D/I_G$  ratios around the middle and end of GW.

On the whole, the adverse effects of longitudinal position as well as acetic acid concentration are in good agreement with FESEM results (Figs 2 and 3). Thus, based upon all the above findings, one may attribute the increased  $I_D/I_G$  ratios to thickening of CNTs arrays by amorphous carbons overcoats.

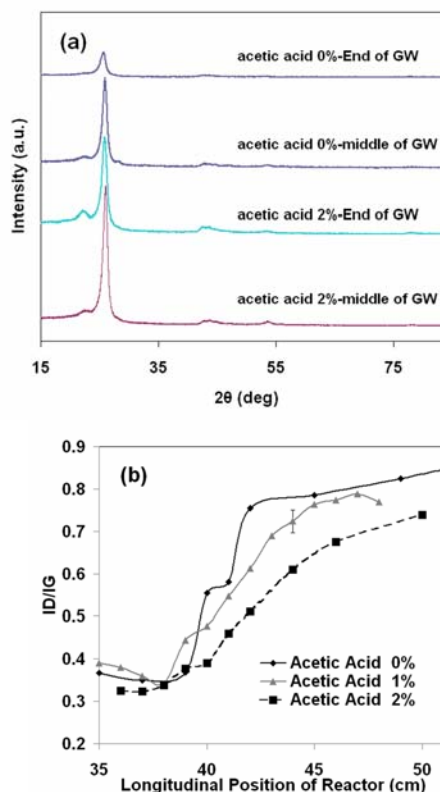


Fig. 4 (a) Typical Raman results of AA0 sample at the beginning, middle and end of GW. (b) Longitudinal variation of the intensity ratio of the D- to G- band ( $I_D/I_G$ ) corresponding to CNTs arrays grown along the GW

### 3.4. Crystallinity of products

Fig. 5 presents X-ray diffraction patterns of AA0 and AA2 samples in two different axial locations of GW. The XRD spectra show that both samples have a quite strong peak at around  $2\theta = 26^\circ$ , known as belonging to graphite (002) plane, and is related to crystallinity of the graphitic layers [32].

One can see from Fig. 5(a) that at the same longitudinal positions, the peak at  $2\theta = 26^\circ$  of AA2 sample has less full width at half maximum (FWHM) than AA0 sample, indicating higher crystalline structure of the former. However, FWHM of both samples increase along the longitudinal positions indicating a drop in crystallinity of the carbon structures from middle toward the end. These findings are consistent with FESEM and Raman spectroscopy results presented in Figs 2-4.

Because of low amount of the catalyst precursor (and so catalyst content of the CNTs), close proximity of diffraction patterns of suspected species (i.e., metallic iron and iron carbide phases), as well as peculiar orientation/strains of catalyst particles inside the graphitic CNTs, it is hard to determine catalyst-related phases. However, our Rietveld refinement suggests probable coexistence of different metallic and carbide phases (Fig. 5(b)).

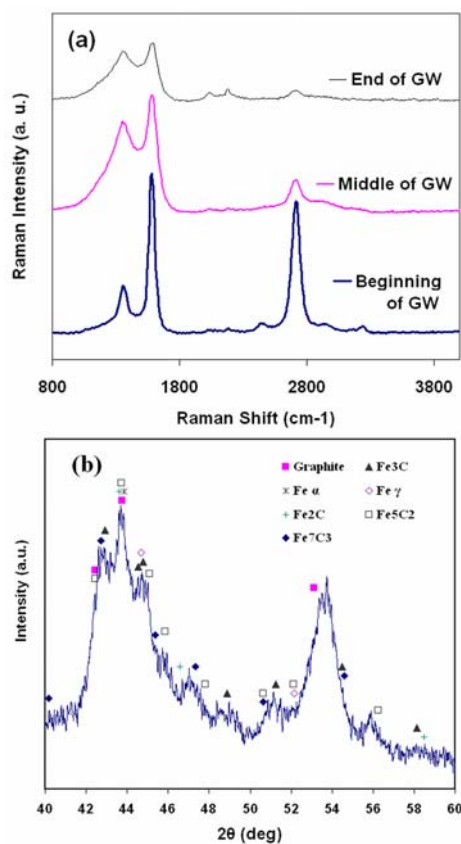


Fig. 5 (a) X-ray diffraction patterns of AA0 and AA2 samples at middle and end of GWs. (b) The typical peaks around  $2\theta = 40-65^\circ$ , related to catalyst-based phases for the case of AA2 sample around the middle of GW

### 3.5. Internal nanostructures of CNTs

Fig. 6 illustrates high-resolution micrographs of CNTs grown at the middle of GW of AA0 and AA2 samples. The AA2 sample (Fig. 6(a)) comprises several graphene layers, with few amorphous/irregular structures on the outer wall. On the other hand, AA0 sample (Fig. 6(b)) includes fewer graphitic walls, covered by a thick amorphous coating. One also can observe amorphous overcoat peeled away from graphitic layers, suggesting again brittle nature of the former.

The less amorphous coating of AA2 sample compared to that in AA0 sample confirms the results obtained by FESEM and Raman spectroscopy, i.e. Figs. 2-4. The larger number of graphene walls of AA2 sample compared with corresponding image of AA0 sample is also in accordance with XRD results, i.e. Fig. 5, which showed more crystalline carbon in the former. It may also points to a more competitive catalytic deposition in AA2 sample, which not only results in longer CNTs arrays (Fig. 1(a)), but also thicker graphitic layers.

The internal diameters of CNTs as well as graphene interlayer distance were found to be about 7-12 and 0.34-0.36 nm respectively, with insignificant changes between AA0 and AA2 samples. One can also see bamboo structure, which is placed just next to the catalyst particle (Fig. 6(a)).

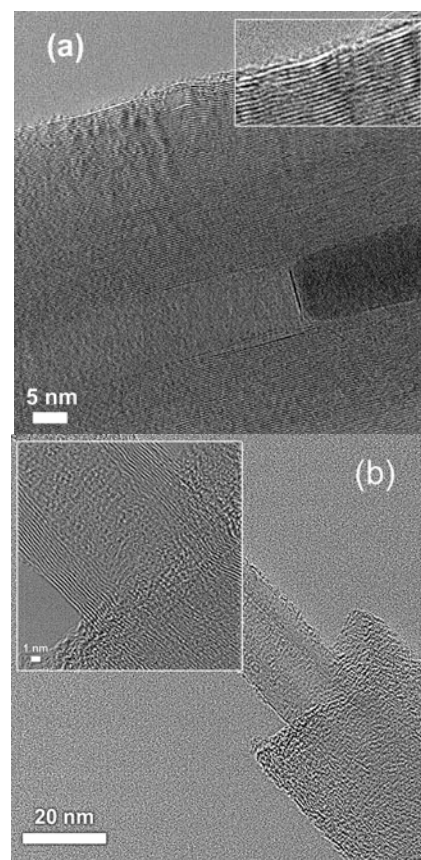


Fig. 6 High resolution TEM micrographs of CNTs grown on the middle of GWs of AA2 (a) and AA0 (b) samples

### 3.6. Analysis of heavy byproducts

In order to gain deeper insight about amorphous carbon, we investigated the formation of heavy byproducts, believed to be precursors of amorphous carbon [33-35]. Analysis of the solid residues by HPLC, confirmed the presence of some PAHs. As can be seen in Fig. 7(a), a number of 3, 4, and 5-ring PAHs were identified in the solid residues. Due to the vacuum drying protocol for sample preparation, we failed to identify relatively low boiling-point and lighter components such as naphthalene. However, the development of 3- to 5-ring PAHs may suggest successive increment of ring number [36]. This may be due to stepwise growth of PAHs through hydrogen abstraction acetylene addition mechanism (HACA) [25, 37].

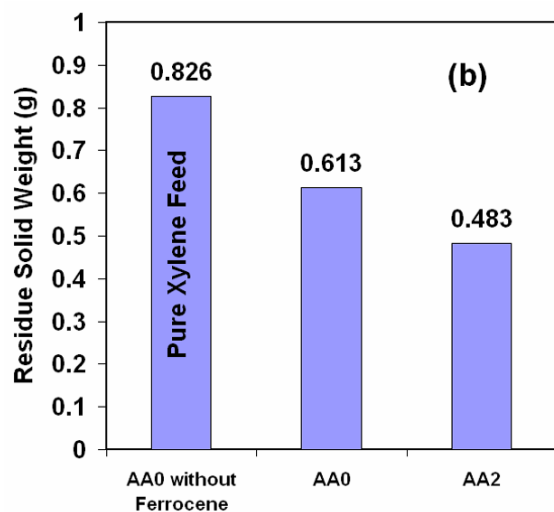
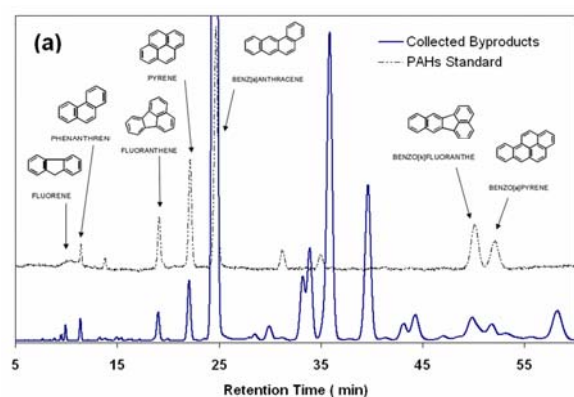


Fig. 7 (a) A typical HPLC result of heavy byproducts of CNTs synthesis for the case of pure xylene feed, compared with PAHs standard mixture. For the sake of clarity, the quite similar patterns were not shown for the cases of AA0 and AA2. (b) The total solid weight extracted by dichloromethane from the reactor and steel condenser at the end of synthesis of AA0 and AA2 samples, as well as pure xylene feed

The total weights of solid residues are presented in Fig. 7(b) for AA0, AA2 and pure xylene feed. In the case of latter, which predictably cause no catalytic growth, the highest residue weight is observed. However, the residue weight decrease after successive improvement of catalytic growth resulted from addition of catalyst precursor as well as acetic acid (Fig. 1(a)). As can be seen, faster catalytic growth reactions can be related to reduction of PAHs. It may be due to the consumption/reduction of precursors of PAHs.

As stated before,  $C_2$  hydrocarbons are more competitive in catalytic reactions than xylene itself. On the other hand,  $C_2$  hydrocarbons can also result in heavy products PAHs, via HACA mechanism [25, 37]. Thus, small amount of  $C_2$  hydrocarbons (most importantly acetylene) can be a competitive source for both catalytic and thermal reactions. These intermediates may be catalytically consumed more rapidly in effect of acetic acid. It was suggested that resultant  $CO_2$  can inhibit the amorphous carbon deposition [11]. The less amorphous carbon can be interpreted as less inhibition and so higher catalytic turnover, which in turn can reduce  $C_2$  hydrocarbons. The lower  $C_2$  hydrocarbons may explain the observed reduction of PAHs (Fig. 7(b)) as well as of PAHs product, i.e. amorphous carbon (Fig. 4(b)). Thus the inhibition of amorphous carbon deposition on catalyst surface can again result in lower production of amorphous carbon. In the other word, just small amount of acetic acid can significantly reduce amorphous carbon content.

### 4. Conclusion

Point-to-point investigation of graphitic CNTs as well as amorphous species has been employed throughout the GW. It was found that increased temperature and residence time along this region, gradually increase the catalytic growth rate, but it also result in more thermally-developed light and heavy byproducts. The former (such as secondary  $C_2$  hydrocarbons and namely acetylene) may promote both the catalytic CNTs growth as well as pyrolytic development of the latter (namely PAHs), which may later develop to amorphous carbon. The amorphous carbon was found to increase the outer diameter of CNTs, and to gradually inhibit the catalytic growth of CNTs, leading to gradual termination of GW.

Acetic acid additive was revealed to reduce amorphous carbon overcoat and the catalyst inhibition, resulting in longer CNTs, with more graphitic layers. It was also shown that acetic acid can reduce probable precursor of amorphous carbon, i.e., PAHs. Thus, we suggest the negative effect of acetic acid on amorphous carbon and PAHs to be related to reduction of their precursors (i.e.,  $C_2$  hydrocarbon), due to their competitively higher catalytic consumption.

### Acknowledgement

M. Maghrebi would like to thank Mohammad Ghaffari, Stevin Snellius Pramana and Hosnieh Sahebkar.

## References

- [1] O. Breuer, U. Sundararaj, *Polym Compos* **25**, 630 (2004).
- [2] R. Vajtai, B. Q. Wei, P. M. Ajayan, *Philos Trans R Soc Lond Ser A-Math Phys Eng Sci* **362**, 2143 (2004).
- [3] Z. J. Zhang, C. Dewan, S. Kothari, S. Mitra, D. Teeters, *Mater Sci Eng B-Solid State Mater Adv Technol* **116**, 363 (2005).
- [4] Z. E. Horvath, K. Kertesz, L. Petho, A. A. Koos, L. Tapasztó, Z. Vertesy, Z. Osvath, A. Darabont, P. Nemes-Incze, Z. Sarkozi, L. P. Biro, *Curr Appl Phys* **6**, 135 (2006).
- [5] N. Sonoyama, M. Ohshita, A. Nijubu, H. Nishikawa, H. Yanase, J. Hayashi, T. Chiba, *Carbon* **44**, 1754 (2006).
- [6] W. G. Zhang, H. M. Cheng, G. Su, Y. Y. Fan, F. Li, Z. H. Shen, B. L. Zhou, *J Mater Sci Technol* **15**, 1 (1999).
- [7] D. H. Kuo, M. Y. Su, W. R. Chen, *Chem Vapor Depos* **12**, 395 (2006).
- [8] W. Wasel, K. Kuwana, P. T. A. Reilly, K. Saito, *Carbon* **45**, 833 (2007).
- [9] G. Y. Zhang, D. Mann, L. Zhang, A. Javey, Y. M. Li, E. Yenilmez, Q. Wang, J. P. McVittie, Y. Nishi, J. Gibbons, H. J. Dai, *Proc Nat Acad Sci USA* **102**, 16141 (2005).
- [10] M. Chen, Y. C. Kao, H. W. Yu, S. C. Lu, H. S. Koo, *Thin Solid Films* **516**, 277 (2007).
- [11] Q. Wen, W. Z. Qian, F. Wei, Y. Liu, G. Q. Ning, Q. Zhang, *Chem Mater* **19**, 1226 (2007).
- [12] Y. L. Li, I. A. Kinloch, A. H. Windle, *Sci* **304**, 276 (2004).
- [13] F. Lupo, J. A. Rodriguez-Manzo, A. Zamudio, A. L. Elias, Y. A. Kim, T. Hayashi, M. Muramatsu, R. Kamalakaran, H. Terrones, M. Endo, M. Ruhle, J. Terrones, *Chem Phys Lett* **410**, 384 (2005).
- [14] S. Musso, S. Porro, M. Rovere, A. Chiodoni, A. Tagliaferro, *Diam Relat Mater* **16**, 1174 (2007).
- [15] S. Porro, S. Musso, M. Giorcelli, A. Chiodoni, A. Tagliaferro, *Physica E: Low-dimens Syst Nanostruct* **37**, 16 (2007).
- [16] Y. F. Liu, Z. M. Shen, B. H. Ma, J. M. Yu, *New Carbon Mater* **18**, 295 (2003).
- [17] D. C. Lee, F. V. Mikulec, B. A. Korgel, *J Amer Chem Soc* **126**, 4951 (2004).
- [18] K. Yamada, M. Tanaka, F. Nakagawa, N. Yoshida, *Rapid Comm Mass Spectrom* **16**, 1059 (2002).
- [19] A. Moiala, A. G. Nasibulin, D. P. Brown, H. Jiang, L. Khriachtchev, E. I. Kauppinen, *Chem Eng Sci* **61**, 4393 (2006).
- [20] S. Chaisitsak, J. Nukeaw, A. Tuantranont, *Diam. Relat. Mat.* **16**, 1958 (2007).
- [21] A. Chauvel, and G. Lefebvre, *Petrochemical Processes*, Edition Technip, Paris (1989).
- [22] R. D. Kamachali, *Chem Phys* **327**, 434 (2006).
- [23] R. I. Masel, *Chemical Kinetics and Catalysis*, John Wiley & Sons, Inc., New York (2001).
- [24] K. Kuwana, H. Endo, K. Saito, D. L. Qian, R. Andrews, E. A. Grulke, *Carbon* **43**, 253 (2005).
- [25] K. Kuwana, T. X. Li, K. Saito, *Chem Eng Sci* **61**, 6718 (2006).
- [26] A. Morancais, B. Caussat, Y. Kihn, P. Kalck, D. Plee, P. Gaillard, D. Bernard, P. Serp, *Carbon* **45**, 624 (2007).
- [27] P. Ramesh, N. Kishi, T. Sugai, H. Shinohara, *J Phys Chem B* **110**, 130 (2006).
- [28] B. W. Jeong, J. K. Lim, S. B. Sinnott, *Appl Phys Lett* **90**, 231021 (2007).
- [29] M. G. Fyta, I. N. Remediakis, P. C. Kelires, D. A. Papaconstantopoulos, *Phys Rev Lett* **96** (2006).
- [30] Q. L. Bao, H. Zhang, C. X. Pan, *Comput Mater Sci* **39**, 616 (2007).
- [31] J. L. Killian, N. B. Zuckerman, D. L. Niemann, B. P. Ribaya, M. Rahman, R. Espinosa, M. Meyyappan, C. V. Nguyen, *J Appl Phys* **103** (2008).
- [32] A. Tanaka, S. H. Yoon, I. Mochida, *Carbon* **42**, 591 (2004).
- [33] G. L. Dong, K. J. Huttinger, *Carbon* **40**, 2515 (2002).
- [34] Z. J. Hu, W. G. Zhang, K. J. Huttinger, B. Reznik, D. Gerhtsen, *Carbon* **41**, 749 (2003).
- [35] G. F. Glasier, R. Filfil, P. D. Pacey, *Carbon* **39**, 497 (2001).
- [36] K. Lombaert, L. Le Moyne, J. T. De Maleissye, J. Amouroux, *Combust Sci Technol* **178**, 707 (2006).
- [37] V. V. Kislov, A. M. Mebel, *J Phys Chem A* **111**, 3922 (2007).

\*Corresponding author: maghrebi@ut.ac.ir